Two-dimensional dynamics of the plasma wakefield accelerator

Rhon Keinigs, and Michael E. Jones

Citation: The Physics of Fluids **30**, 252 (1987); doi: 10.1063/1.866183
View online: https://doi.org/10.1063/1.866183
View Table of Contents: http://aip.scitation.org/toc/pfl/30/1
Published by the American Institute of Physics

Two-dimensional dynamics of the plasma wakefield accelerator

Rhon Keinigs and Michael E. Jones
Applied Theoretical Physics Division, Los Alamos National Laboratory, Los Alamos, New Mexico, 87545

(Received 11 April 1986; accepted 6 October 1986)

A general analysis of the electromagnetic wakefields for an axisymmetric charge distribution moving through a cold uniform plasma is presented. Particular attention is given to the electromagnetic and relativistic effects influencing the waves. It is shown that the plasma provides shielding of the transverse wakefields on a scale length of a few electromagnetic skin depths (c/ω_p). The implications for plasma wakefield accelerators are that driving beams with radii of a few skin depths will experience severe pinching, whereas larger beams will be subject to filamentation instabilities. These conclusions are supported by self-consistent particle-in-cell simulations. The deleterious effects of transverse wakefields will severely limit the accelerating gradients that can be obtained even if a magnetic field is used to guide the driving beam.

I. INTRODUCTION

In this paper we present an investigation of the two-dimensional dynamics of the plasma wakefield accelerator (PWFA).[1] The PWFA is an advanced accelerator concept that is based on utilizing a large amplitude plasma wave to accelerate relativistic electrons to ultrahigh energies (TeV or higher). The wave acts as an intermediary or transformer, extracting energy from a driving beam and transferring it into a trailing group of electrons. Chen *et al.*[1] were first to discuss this concept: Using an electrostatic one-dimensional model and particle-in-cell simulations they showed how such a wave is excited by a single relativistic electron, and demonstrated that acceleration of a trailing electron bunch is possible. Estimates based on wave-breaking limits result in accelerating gradients on the order of 10 GeV/m in a plasma of density, $n_p = 10^{17}\,\mathrm{cm}^{-3}$ ($E_a \propto n_p^{1/2}$ eV/cm). Two-dimensional electrostatic calculations indicate that the radial electric field can be used to focus the trailing bunch.[2]

The plasma wave, which has a phase velocity near c, actually represents the wake produced by a relativistic charged particle or beam as it passes through a cold plasma. Because the wave serves as a transformer it indicates that using a high current beam as a driver could improve the efficiency of such an accelerator. In fact, using a high current beam allows one to achieve a large transformer ratio. The transformer ratio is the ratio of two electric fields, the maximum accelerating field behind the driving beam and the maximum decelerating field within the beam, $R \equiv E_a/E_d$. To have an efficient wakefield accelerator one must make R large. In order to accomplish this it is necessary that the beam give up all its energy to the wakefield. This means that the field seen by the beam should be wholly decelerating. If for example, the tail of the beam gets accelerated by the wakefield, then R will be less than its optimal value. Until recently it was believed that R could not exceed two in a colinear device.[3] This fundamental theorem of beam loading, as it is known, is based on the assumption that the current distribution of the driving beam is symmetric head to tail. Bane *et al.*[4] have circumvented this theorem and demonstrated that large transformer ratios can be achieved by properly ramping the beam current. (The first detailed analysis considering asymmetric driving beams was provided by Chen and Dawson.[5]) This important breakthrough provides the motivation for a detailed electromagnetic analysis of the plasma wakefield accelerator. The model problem treated by Bane was electrostatic and therefore did not include two-dimensional effects such as beam pinching. To attempt to address the questions of how the wakefield affects the self-consistent radial dynamics of the beam and how this in turn affects the PWFA, we have carried out a fully electromagnetic, two-dimensional analysis.

The paper is divided into three main sections. In Sec. II we give a formal, electromagnetic, and fully relativistic derivation of the electric and magnetic fields that are generated by an azimuthally symmetric current distribution passing through a cold, unmagnetized plasma. The three field components that are calculated are E_z, E_r, and B_θ. Here E_r and B_θ are combined to form what we refer to as the radial wakefield, $\mathbf{W} = \mathbf{r}(E_r - \beta B_\theta)$; $\mathbf{W}$ acts to pinch the driving beam. The current distribution is assumed to be an arbitrary function of radius and the variable $y = v_b t - z$, where v_b defines the beam velocity. We will write the beam current in terms of the beam charge density $j_b(r,y) = \beta c \rho_b(r,y)\mathbf{z}$, where $\beta = v_b/c$, and when convenient we will interchange $\rho_b(r,y)$ with its separated form, $\sigma(r)f(y)$. For the analytic treatment we consider the case of an ultrarelativistic beam, meaning that v_b can be treated as constant; not until the beam loses a significant amount of energy to the wakefield does v_b change appreciably. In the numerical simulations of the final section v_b is allowed to change.

Two methods for calculating these fields are presented in Sec. II. The first approach involves Fourier transforming in the variable y and using the radial Green's functions for Bessel's operator to get the Fourier-transformed fields. Inverse Fourier transforming requires the integration around branch cuts, and if this is not handled carefully incorrect fields will result. We demonstrate how this can occur if the infinite γ limit is taken before the inverse transformation is performed. The correct fields, which reduce to the proper vacuum fields, are obtained using the second approach, which employs a Hankel transform in the radial variable. We check the results using this method by considering the case of a relativistic point particle, and showing that the

 0031-9171/87/010252-12$01.90

fields are the same as those derived by Fermi in calculating the energy loss of a particle passing through a plasma (the so-called "density effect").[6]

In Sec. III we extend the analysis to include continuous current distributions, and evaluate the fields for two particular choices for the axial beam profile $f(y)$; a uniform current profile and one that corresponds to the "doorstep" transformer ratio. The radial wakefield for these distributions is also evaluated. We find the interesting result that the current profile yielding the larger transformer ratio results in the largest magnetic self-pinching of the driving beam. There is a subtle reason why this is so: The doorstep current profile produces an induced charge density that exactly cancels the repulsive radial space charge field of the beam. There is then nothing to counteract the magnetic pinching attributable to the beam current. Once the beam pinches the current profile is altered and the transformer ratio is reduced.

After pinching has begun the evolution of the beam is very nonlinear, and can only be followed numerically. This is done in Sec. IV. As we show in this section beam pinching can be severe for small radii beams. This leads to a deterioration of the acceleration mechanism, as is displayed in the simulation results found using ISIS,[7] a fully relativistic, electromagnetic particle-in-cell model. We find that deleterious pinching can only be avoided if the beam is broad (many plasma wavelengths across), in which case the current necessary to drive a useful PWFA is excessively large and subject to filamentation instabilities. The strong and weak pinching we find for the different radii beams can be attributed to a difference in the return current induced in the plasma for the two cases. We end Sec. IV by giving some requirements on the beam current and geometry that are necessary to yield an accelerating gradient for the PWFA that is comparable to that which can be obtained using conventional rf technology. From these estimates we conclude that a useful plasma wakefield accelerator can only be operated if immersed in a strong magnetic field.

II. DETERMINATION OF THE ZERO-ORDER WAKEFIELD

The derivation that follows is a zero-order analysis of the wakefields, i.e., we do not self-consistently treat the radial motion of the beam dynamics that results from the fields generated within the plasma. This means that the beam current remains unaltered during the evolution of the fields. This is a valid approximation for a time on the order of a beam plasma period, but breaks down after this as a result of self-pinching of the beam. The ions are considered to be immobile.

There are many ways in which one can derive the wakefields. Previous authors have solved for the fields by first obtaining the vector and scalar potentials. Cox and Bennett used this approach in some of the earliest work pertaining to the generation of a plasma wakefield.[8] They were interested in calculating the return current induced in a relativistic electron beam as it traveled through a cold background plasma. Using a two-dimensional current profile of the form $j_z(r,z,t) = \sigma(r) f(v_b t - z)$ they obtained the electrostatic field generated by the beam, and noted that this field was oscillatory. Cox and Bennett were not, however, interested in using the electric field for acceleration purposes, so no particular forms for $f(y)$ were considered in their work. We elect to solve directly for the fields.

We begin by considering the wave equations for the vector and scalar potentials; in the Lorentz gauge these are

$$\left(\nabla^2 - \frac{1}{c^2}\frac{\partial^2}{\partial t^2}\right)\mathbf{A}(\mathbf{r},t) = -\frac{4\pi}{c}\mathbf{j}(\mathbf{r},t), \tag{1}$$

$$\left(\nabla^2 - \frac{1}{c^2}\frac{\partial^2}{\partial t^2}\right)\Phi(\mathbf{r},t) = -4\pi\rho(\mathbf{r},t). \tag{2}$$

A corresponding wave equation for the electric field, $\mathbf{E} = -[\nabla\Phi + (1/c)(\partial/\partial t)\mathbf{A}]$ can be obtained from these equations by operating on Eq. (1) with $(1/c)\partial/\partial t$ and Eq. (2) with ∇ and adding;

$$\left(\nabla^2 - \frac{1}{c^2}\frac{\partial^2}{\partial t^2}\right)\mathbf{E}(\mathbf{r},t) = \frac{4\pi}{c^2}\frac{\partial}{\partial t}\mathbf{j} + 4\pi\nabla\rho. \tag{3}$$

We want to reduce this equation to an inhomogeneous equation for $\mathbf{E}$ with the source term being a function of the beam parameters alone. We can do this by separating the source term in Eq. (3) into two pieces, an external beam contribution, which we will represent with the subscript b, and an induced plasma response, which we will denote with a subscript p. We can then use Ohm's law to eliminate the plasma current from the rhs of Eq. (3) in favor of $\mathbf{E}$ to obtain

$$\left(\nabla^2 - \frac{\omega_p^2}{c^2} - \frac{1}{c^2}\frac{\partial^2}{\partial t^2}\right)\mathbf{E} = \frac{4\pi}{c^2}\frac{\partial}{\partial t}\mathbf{j}_b + 4\pi\nabla\rho_{\text{tot}}, \tag{4}$$

where $\rho_{\text{tot}} = \rho_b + \rho_p$, and $\omega_p = (4\pi e^2 n_p/m)^{1/2}$ is the plasma frequency of the background; n_p is the plasma density and m is the electron mass. A similar equation for the magnetic field is obtained by taking the curl of Eq. (4) and using Faraday's law, $\nabla\times\mathbf{E} = -(1/c)(\partial/\partial t)\mathbf{B}$;

$$\left(\nabla^2 - \frac{\omega_p^2}{c^2} - \frac{1}{c^2}\frac{\partial^2}{\partial t^2}\right)\mathbf{B} = -\frac{4\pi}{c}\nabla\times\mathbf{j}_b. \tag{5}$$

Note that the source term for the magnetic field depends only upon the beam current. This means that the induced plasma perturbation results in a purely electrostatic plasma response. Therefore no electromagnetic radiation will be generated by the beam.

The equations are now rewritten assuming that all axial and temporal dependencies enter only through the combination of variables, $v_b t - z$. Defining the change of variable, $y = v_b t - z$, and considering the source to be azimuthally symmetric, the equations for the fields become

$$\left(\Delta - k_0^2 + \frac{1}{\gamma^2}\frac{\partial^2}{\partial y^2}\right)\mathbf{E} = -\mathbf{z}4\pi\frac{\partial}{\partial y}\left(\frac{\rho_b}{\gamma^2} + \rho_p\right) + \mathbf{r}4\pi\frac{\partial}{\partial r}(\rho_b + \rho_p), \tag{6}$$

$$\left(\Delta - k_0^2 + \frac{1}{\gamma^2}\frac{\partial^2}{\partial y^2}\right)\mathbf{B} = \boldsymbol{\theta}4\pi\beta\frac{\partial}{\partial r}\rho_b. \tag{7}$$

Here we have substituted $j_b = \beta c\rho_b$, $\gamma = (1-\beta^2)^{-1/2}$, and have defined $\Delta = \nabla^2 - \partial^2/\partial z^2$. The equation for the radial wakefield, $\mathbf{W} = \mathbf{r}(E_r - \beta B_\theta)$, which determines the perpendicular dynamics of the beam, becomes

$$\left(\Delta - k_0^2 + \frac{1}{\gamma^2}\frac{\partial^2}{\partial y^2}\right)\mathbf{W} = \mathbf{r}\frac{\partial}{\partial r}\left(\frac{\rho_b}{\gamma^2} + \rho_b\right). \tag{8}$$

From these equations one can say several things about the resulting fields given particular forms for the source terms. For example, if $\rho_b/\gamma^2 + \rho_p$ is a linear function of y within the beam, then E_z is uniform within the beam and $|\mathbf{W}|$ increases linearly from head to tail. In like manner E_r can be made to vanish within the beam if $\rho_b + \rho_p$ can be made to vanish. Beam profiles resulting in these characteristics can be found and are the subject of Sec. III.

To solve these equations we first Fourier transform in y. Defining k to be the transform variable we obtain

$$\left[\Delta - \left(k_0^2 + \frac{k^2}{\gamma^2}\right)\right]\hat{\mathbf{E}}(\mathbf{r},k) = \mathbf{z}i4\pi k\left(\frac{\hat{\rho}_b(r,k)}{\gamma^2} + \hat{\rho}_p(r,k)\right) + \mathbf{r}4\pi\frac{\partial}{\partial r}(\hat{\rho}_b + \hat{\rho}_p), \tag{9}$$

$$\left[\Delta - \left(k_0^2 + \frac{k^2}{\gamma^2}\right)\right]\hat{\mathbf{B}}(r,k) = \boldsymbol{\theta}4\pi\beta\frac{\partial}{\partial r}\hat{\rho}_b(r,k). \tag{10}$$

Carets denote the Fourier-transformed fields. There is a corresponding equation for the transformed wakefield $\mathbf{W}$. To get the equations in their final form we need to express the induced plasma charge density $\hat{\rho}_p(r,k)$ in terms of the source, $\hat{\rho}_b(r,k)$. The following equation relating $\rho_p(r,y)$ to $\rho_b(r,y)$ can be derived using the linearized continuity and momentum equations for the plasma electrons combined with Poisson's equation relating $\mathbf{E}$ to the total charge density:

$$\frac{\partial^2}{\partial y^2}\rho_p + k_p^2\rho_p = -k_p^2\rho_b. \tag{11}$$

Here we have defined the wave vector $k_p = \omega_p/v_b$. Linearization implies that the analysis is only valid provided that the beam density $n_b \ll n_p$. Fourier transforming yields $\hat{\rho}_p(r,k)$,

$$\hat{\rho}_p(r,k) = [k_p^2/(k^2 - k_p^2)]\hat{\rho}_b(r,k). \tag{12}$$

Substituting Eq. (12) into Eqs. (9) and (10) we obtain our final set of equations for the Fourier-transformed fields,

$$\left[\Delta - \left(k_0^2 + \frac{k^2}{\gamma^2}\right)\right]\hat{\mathbf{E}}(\mathbf{r},k) = \mathbf{z}i4\pi k\frac{k^2/\gamma^2 + k_0^2}{k^2 - k_p^2}\hat{\rho}_b(r,k) + \mathbf{r}4\pi\frac{k^2}{k^2 - k_p^2}\frac{\partial}{\partial r}\hat{\rho}_b, \tag{13}$$

$$\left[\Delta - \left(k_0^2 + \frac{k^2}{\gamma^2}\right)\right]\hat{\mathbf{B}}(r,k) = \boldsymbol{\theta}4\pi\beta\frac{\partial}{\partial r}\hat{\rho}_b(r,k). \tag{14}$$

At this point there are two approaches one may take in finding $\Psi(r,y)$. (Here Ψ is used to represent any general field component.) The first, and probably most obvious, involves expressing $\Psi(r,k)$ in terms of a radial Green's function and then inverse Fourier transforming to get $\Psi(r,y)$. This method was used by Cox and Bennett.[8] The second approach utilizes a Hankel transform in the radial variable, and proves simpler when it comes to performing the inverse Fourier transform.

Recognizing the operator on the lhs of the field equations as Bessel's operator gives for the three Fourier-transformed field components:

$$\hat{E}_z(r,k) = 4\pi ik\left(\frac{k^2/\gamma^2 + k_0^2}{k^2 - k_p^2}\right)\int_0^\infty dr'\, r'\hat{\rho}_b(r',k) \times I_0\left(\sqrt{\frac{k^2}{\gamma^2} + k_0^2}\, r_<\right)K_0\left(\sqrt{\frac{k^2}{\gamma^2} + k_0^2}\, r_>\right), \tag{15}$$

$$\hat{E}_r(r,k) = 4\pi\frac{k^2}{k^2 - k_p^2}\int_0^\infty dr'\, r'\frac{\partial}{\partial r}\hat{\rho}_b(r',k) \times I_1\left(\sqrt{\frac{k^2}{\gamma^2} + k_0^2}\, r_<\right)K_1\left(\sqrt{\frac{k^2}{\gamma^2} + k_0^2}\, r_>\right), \tag{16}$$

$$\hat{B}_\theta(r,k) = 4\pi\beta\int_0^\infty dr'\, r'\frac{\partial}{\partial r'}\hat{\rho}_b(r',k) \times I_1\left(\sqrt{\frac{k^2}{\gamma^2} + k_0^2}\, r_<\right)K_1\left(\sqrt{\frac{k^2}{\gamma^2} + k_0^2}\, r_>\right). \tag{17}$$

Within the arguments of the modified Bessel functions $r_<$ and $r_>$, respectively, denote the minimum and maximum of r and r'. Note that $\hat{E}_z(r,k)$ and $\hat{E}_r(r,k)$ have simple poles at $k = \pm k_p$ and branch points at $k = \pm i\gamma k_0$. On the other hand, $\hat{B}_\theta(r,k)$ only contains the branch points at $\pm i\gamma k_0$. The pole contributions correspond to electrostatic plasma waves; in the vacuum limit ($k_p \to 0$) these waves vanish. The branch cut contributions correspond to nonoscillatory electromagnetic components of the field; in the vacuum limit these reduce to the fields generated by a bare beam. The contours used in inverting the Fourier transform of the electric field are shown in Fig. 1. It should be noted that if the branch cuts are not correctly treated one does not obtain the correct radial electric field. As an example, we show how this can occur if one takes the infinite γ limit before performing the branch cut integration. If we let $\gamma \to \infty$ ($k_0 = k_p$) then the branch points recede to $\pm i\infty$, and the arguments of the Bessel functions in Eqs. (15)–(17) go to $k_0(r_<, r_>)$. The

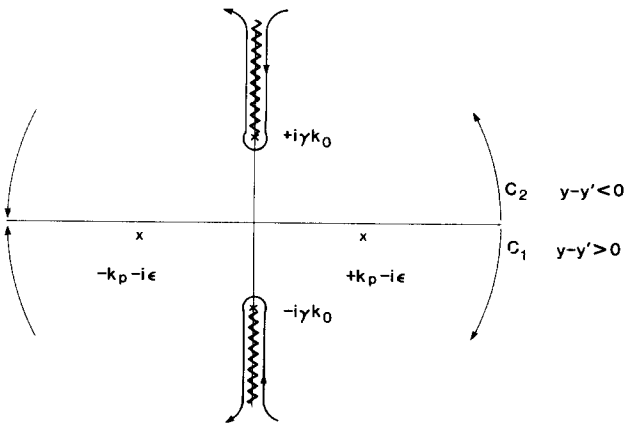

FIG. 1. Contours of integration for evaluating the electric field components given in Eqs. (15) and (16).

Bessel functions can then be factored out of the inversion integrals, and we find for the fields in this limit,

$$E_z(r,y) = -4\pi k_p^2 \int_0^\infty dr'\, r' I_0(k_p r_<) \times \int_0^y dy' \rho_b(r',y') \cos k_p (y-y'), \tag{18}$$

$$E_r(r,y) = 4\pi k_p \int_0^\infty dr'\, r' I_1(k_p r_<) K_1(k_p r_>) \times \int_0^y dy' \frac{\partial}{\partial r'} \rho_b(r',y') \sin k_p (y-y'), \tag{19}$$

$$B_\theta(r,y) = 4\pi\beta \int_0^\infty dr'\, r' \frac{\partial}{\partial r'} \rho_b(r',y') I_1(k_p r_<) K_1(k_p r_>). \tag{20}$$

The integrations over y' in Eqs. (18) and (19) arise from using the convolution theorem for Fourier transforms. In these equations if y is greater than the pulse length, which we shall denote by L, then the upper limit of integration becomes L. In the vacuum limit both E_z and E_r vanish; they do not reduce to the fields for a bare beam. This error is simply avoided if the branch cut integration is performed before the infinite γ limit is taken. To lowest order in γ^{-1} the correct electric fields are given in Eqs. (57)–(59), respectively.

The second approach, which takes into account finite γ, but avoids the necessity of integrating around the branch cuts, employs a Hankel transform in the radial variable. The advantage of this method is that all singularities of the Fourier–Hankel-transformed equations take the form of simple poles. Adopting Sneddon's definition[9] we denote the Hankel transform of a function $\Psi(r)$ by

$$H_\nu(\hat{\Psi}(r,k),\zeta) = \tilde{\Psi}(\zeta,\nu,k) = \int_0^\infty dr\, r \hat{\Psi}(r,k) J_\nu(\zeta r). \tag{21}$$

Tildes will be used to refer to Hankel-transformed functions, and for brevity the ν appearing in $\tilde{\Psi}(\zeta,\nu,k)$ will be dropped. The original function is then given in terms of the inverse transform

$$\hat{\Psi}(r,k) = \int_0^\infty d\zeta\, \zeta J_\nu(\zeta r) \tilde{\Psi}_\nu(\zeta,k). \tag{22}$$

Defining the operator

$$\beta_\nu = \frac{1}{r}\frac{\partial}{\partial r} r \frac{\partial}{\partial r} - \frac{\nu^2}{r^2}$$

and making use of the relation, $H_\nu[\beta_\nu(\Psi),\zeta] = -\zeta^2 H_\nu(\Psi,\zeta)$, in Eqs. (13) and (14) we obtain the Hankel-transformed fields,

$$\tilde{E}_z(k,\zeta) = -4\pi i \frac{k(k^2/\gamma^2 + k_0^2)}{(k^2 - k_p^2)(k^2/\gamma^2 + k_0^2 + \zeta^2)} \times H_0[\rho_b(r,k),\zeta], \tag{23}$$

$$\tilde{E}_r(k,\zeta) = -4\pi \frac{k^2}{(k^2 - k_p^2)(k^2/\gamma^2 + k_0^2 + \zeta^2)} \times H_1\left(\frac{\partial}{\partial r}\rho_b(r,k),\zeta\right), \tag{24}$$

$$\tilde{B}_\theta(r,y) = -4\pi\beta \frac{1}{k^2/\gamma^2 + k_0^2 + \zeta^2} \times H_1\left(\frac{\partial}{\partial r}\rho_b(r,k),\zeta\right). \tag{25}$$

Only simple poles appear on the rhs of these equations, therefore the inverse Fourier transforms can be done easily. In performing the inverse Fourier transforms the poles at $\pm k_p$ are displaced into the lower-half plane an amount, $-i\epsilon$. This represents a finite amount of dissipation in the system. The results for an ideal plasma are recovered after performing the inverse transform by taking the limit, $\epsilon \to 0$. As a simple check of the Hankel transform method we evaluate the Fourier-transformed fields for a point particle on axis; $\rho_b(r,y) = q/2\pi\delta(y)\delta(r)/r$. For this example

$$H_0(\rho_b(r,k),\zeta) = \frac{q}{2\pi}\int_{-\infty}^{\infty} dy\, e^{iky}\delta(y) \times \int_0^\infty dr\, r J_0(\zeta r)\frac{\delta(r)}{r} = \frac{q}{2\pi}, \tag{26}$$

$$H_1\left(\frac{\partial \rho_b}{\partial r},\zeta\right) = -\zeta H_0(\rho_b,\zeta) = -\frac{\zeta q}{2\pi}. \tag{27}$$

Using these expressions in Eqs. (23)–(25) we invert the Hankel transforms to get

$$\hat{E}_z(r,k) = \frac{2iqk(k^2/\gamma^2 + k_0^2)}{(k^2 - k_p^2)} \int_0^\infty d\zeta\, \zeta \frac{J_0(\zeta r)}{k^2/\gamma^2 + k_0^2 + \zeta^2} = \frac{2iqk(k^2/\gamma^2 + k_0^2)}{k^2 - k_p^2} K_0\left(\sqrt{\frac{k^2}{\gamma^2} + k_0^2}\, r\right) \tag{28}$$

(via Gradshteyn and Ryzhik[10]). Similarly,

$$\hat{E}_r(r,k) = \frac{-2qk^2}{k^2 - k_p^2}\sqrt{\frac{k^2}{\gamma^2} + k_0^2}\, K_1\left(\sqrt{\frac{k^2}{\gamma^2} + k_0^2}\, r\right), \tag{29}$$

$$\hat{B}_\theta(r,k) = -2\beta q \sqrt{\frac{k^2}{\gamma^2} + k_0^2}\, K_1\left(\sqrt{\frac{k^2}{\gamma^2} + k_0^2}\, r\right). \tag{30}$$

Equations (28)–(30) are Fermi's expressions for the Fourier transforms of the fields of a point particle moving through a plasma. These are used in calculating the "density effect" for collisional energy losses.[6] We return to calculating the y dependence for these fields later in this section.

We now turn our attention to extended sources. For arbitrary $\rho_b(r,y)$ the convolution theorem for Fourier transforms allows us to write the following [see Eqs. (23)–(25)]:

$$\tilde{E}_z(y,\zeta) = \int_{-\infty}^{\infty} dy'\, H_0[\rho_b(\zeta,y')] G_z(\zeta, y-y'), \tag{31}$$

$$\tilde{E}_r(y,\zeta) = \int_{-\infty}^{\infty} dy'\, H_1\left(\frac{\partial}{\partial r}\rho_b,\zeta\right) G_r(\zeta,y-y'), \tag{32}$$

$$\tilde{B}_\theta(y,\zeta) = \beta \int_{-\infty}^{\infty} dy'\, H_1\left(\frac{\partial}{\partial r}\rho_b,\zeta\right) G_\theta(\zeta,y-y'), \tag{33}$$

where the Green's functions are given by

$$G_z(\zeta,y-y') = 2i\int_{-\infty}^{\infty} dk\, e^{-ik(y-y')} \times \frac{k(k^2/\gamma^2+k_0^2)}{(k^2-k_p^2)(k^2/\gamma^2+k_0^2+\zeta^2)}, \tag{34}$$

$$G_r(\zeta,y-y') = -2\int_{-\infty}^{\infty} dk\, e^{-ik(y-y')} \times \frac{k^2}{(k^2-k_p^2)(k^2/\gamma^2+k_0^2+\zeta^2)}, \tag{35}$$

$$G_\theta(\zeta,y-y') = -2\int_{-\infty}^{\infty} dk\, e^{-ik(y-y')} \times \frac{1}{k^2/\gamma^2+k_0^2+\zeta^2}. \tag{36}$$

The contours for evaluating the Green's functions are closed in the LHP, for $y-y'>0$, and for $y-y'<0$ they are closed in the UHP. Performing the integrations yields

$$G_z(\zeta,y-y') = 4\pi\Theta(y-y')\frac{k_p^2}{k_p^2+\zeta^2}\cos k_p(y-y') + 2\pi\Theta(y-y')\frac{\zeta^2}{k_p^2+\zeta^2}\exp\left[-\gamma\sqrt{k_0^2+\zeta^2}(y-y')\right] - 2\pi\Theta(y'-y)\frac{\zeta^2}{k_p^2+\zeta^2}\exp\left[\gamma\sqrt{k_0^2+\zeta^2}(y-y')\right], \tag{37}$$

$$G_r(\zeta,y-y') = \pi\Theta(y-y')\frac{k_p^2}{k_p^2+\zeta^2}\sin k_p(y-y') - 2\pi\gamma\frac{\sqrt{k_0^2+\zeta^2}}{k_p^2+\zeta^2}\exp(-\gamma\sqrt{k_0^2+\zeta^2}|y-y'|), \tag{38}$$

$$G_\theta(\zeta,y-y') = 2\pi\frac{\gamma\beta}{\sqrt{k_0^2+\zeta^2}}\exp(-\gamma\sqrt{k_0^2+\zeta^2}|y-y'|). \tag{39}$$

Here Θ defines the Heaviside step function. Substituting Eqs. (37)–(39) into Eqs. (31)–(33) and inverse-Hankel transforming yields the fields generated by an arbitrary current distribution, $j_b(r,y)$. In obtaining the following results we have interchanged integrations over r' and ζ and performed the ζ integration first, using the identity[10]

$$I_\nu(k_p r_<)K_\nu(k_p r_>) = \int_0^\infty d\zeta \frac{\zeta}{k_p^2+\zeta^2} J_\nu(\zeta r_<)J_\nu(\zeta r_>).$$

The following fields are fully general:

$$E_z(r,y) = 4\pi k_p^2\int_0^\infty dr'\, r' I_0(k_p r_<)K_0(k_p r_>)\int_0^y dy'\,\rho_b(r',y')\cos k_p(y-y') + 2\pi\gamma\int_0^\infty dr'\,\gamma'\int_0^\infty d\zeta\frac{\zeta^3}{k_p^2+\zeta^2}J_0(\zeta r_<) \times J_0(\zeta r_>)\left(\int_{-\infty}^y dy'\rho_b(r',y')\exp\left[-\gamma\sqrt{k_0^2+\zeta^2}(y-y')\right] - \int_y^\infty dy'\,\rho_b(r',y')\exp\left[\gamma\sqrt{k_0^2+\zeta^2}(y-y')\right]\right), \tag{40}$$

$$E_r(r,y) = 4\pi k_p\int_0^\infty dr'\, r' I_1(k_p r_<)K_1(k_p r_>)\int_0^y dy'\frac{\partial}{\partial r'}\rho_b(r',y')\sin k_p(y-y') - 2\pi\beta\gamma\int_0^\infty dr'\, r'\int_0^\infty d\zeta\,\zeta\frac{\sqrt{k_0^2+\zeta^2}}{k_p^2+\zeta^2}J_1(\zeta r_<)J_1(\zeta r_>)\int_{-\infty}^\infty dy'\frac{\partial}{\partial r'}\rho_b(r',y')\exp(-\gamma\sqrt{k_0^2+\zeta^2}|y-y'|), \tag{41}$$

$$B_\theta(r,y) = 2\pi\beta\gamma\int_0^\infty dr'\, r'\int_0^\infty d\zeta\frac{\zeta}{\sqrt{k_0^2+\zeta^2}}J_1(\zeta r_<)J_1(\zeta r_>)\int_{-\infty}^\infty dy'\frac{\partial}{\partial r'}\rho_b(r',y')\exp(-\gamma\sqrt{k_0^2+\zeta^2}|y-y'|). \tag{42}$$

For the case of an ultrarelativistic beam $k_0 \cong k_p$, and we find for the radial wakefield,

$$W(r,y) = 4\pi k_p\int_0^\infty dr'\, r' I_1(k_p r_<)K_1(k_p r_>)\int_{-\infty}^y dy'\frac{\partial}{\partial r'}\rho_b(r',y')\sin k_p(y-y') - \frac{2\pi}{\gamma}\int_0^\infty dr'\, r'\int_0^\infty d\zeta\frac{\zeta}{\sqrt{k_0^2+\zeta^2}}J_1(\zeta r_<)J_1(\zeta r_>)\int_{-\infty}^\infty dy'\frac{\partial}{\partial r'}\rho_b(r',y')\exp(-\gamma\sqrt{k_0^2+\zeta^2}|y-y'|). \tag{43}$$

In the vacuum limit Eqs. (40)–(42) yield the fields of a bare beam. As a check of this we again consider the case of a point particle. For the point particle, closed form expressions for E_r and B_θ can be obtained and an approximate expression for E_z can

be found. Substituting $\rho_b(r,y) = (q/2\pi)\delta(y)\delta(r)/r$ into Eqs. (40)–(42) yields

$$E_z(r,y) = \Theta(y)\left[2qk_p^2 K_0(k_p r)\cos k_p y - q\frac{\exp[k_p(\gamma y - \sqrt{\gamma^2 y^2 + r^2})]}{\gamma^2 y^2 + r^2}\left(k_p - \frac{\gamma k_p y}{\sqrt{\gamma^2 y^2 + r^2}} - \frac{\gamma y}{\gamma^2 y^2 + r^2}\right)\right]$$
$$+ \Theta(-y)q\frac{\exp[-k_p(\gamma y + \sqrt{\gamma^2 y^2 + r^2})]}{\sqrt{\gamma^2 y^2 + r^2}}\left(k_p + \frac{\gamma k_p y}{\sqrt{\gamma^2 y^2 + r^2}} + \frac{\gamma y}{\gamma^2 y^2 + r^2}\right), \tag{44}$$

$$E_r(r,y) = -\Theta(y)qk_p^2 K_1(k_p r)\sin k_p(y) + \frac{q\gamma r}{\gamma^2 y^2 + r^2}\exp[-k_p(\sqrt{\gamma^2 y^2 + r^2} - \gamma|y|)]\left(k_p + \frac{1}{\sqrt{\gamma^2 y^2 + r^2}}\right), \tag{45}$$

$$B_\theta(r,y) = \frac{q\beta\gamma r}{\gamma^2 y^2 + r^2}\exp[-k_p(\sqrt{\gamma^2 y^2 + r^2} - \gamma|y|)]\left(k_p + \frac{1}{\sqrt{\gamma^2 y^2 + r^2}}\right). \tag{46}$$

The plasma response to the test charge results in an oscillatory field behind the particle. This electrostatic wave has radial and axial components that are 90° out of phase. The axial field can be used to accelerate a trailing charge bunch while the radial field can be employed to focus this bunch. By writing $k_p y = k_p(v_b t - z)$ one sees that the phase velocity for the wave is equal to the beam velocity. The electromagnetic components of the field are shielded by the plasma: in the radial direction these fields fall off exponentially in a plasma skin depth $\lambda_s = c/\omega_p$. In the axial direction they are shielded in a characteristic length given by the relativistic skin depth λ_s/γ. The reduced shielding length in this direction is attributable to the Lorentz contraction and subsequent increase in plasma density along the direction of the beam's motion. All the above fields reduce to the correct vacuum fields in the limit $k_p \to 0$.[6]

In the following section we consider extended current distributions that are relevant to the plasma wakefield accelerator.

III. WAKEFIELDS FOR SPECIFIC CHOICES OF *f(y)*

In order to access the viability of the plasma wakefield accelerator concept one must be able to analyze how different current profiles are going to affect the pinching of the beam. Pinching along the beam will change the current profile, and this in turn will affect the transformer ratio. Also, severe pinching may result in a serious deterioration of the beam's integrity.

In considering specific current profiles we assume that in all cases the current is cut off in a time that is short compared to the inverse plasma frequency of the background. A physical explanation of why such a sharp tailoring at the beam tail is important and how this excites a plasma wake has been given by Chen and Dawson[5] (see also Katsouleas[11]): As the beam enters the plasma the plasma electrons are displaced so as to cancel out the large space charge of the beam. Once the beam tail passes, provided the current is cut off sharply, a large induced charge is left in the plasma,and this locally oscillates at the plasma frequency creating the wakefield. The disturbance follows along behind the beam, hence the wave has a phase velocity equal to the beam velocity. If the beam current is cut off in a time that is longer than a plasma period, then the plasma electrons will have time to adiabatically relax back to their unperturbed positions, and the wakefield will be largely degraded. The requirement for such a sharp cutoff ($T_c < 10^{-12}$ sec for $n_p = 10^{17}$ cm^{-3}) puts a very severe limitation on doing any experiment aimed at generating GeV/m accelerating gradients. However an experimental proof of principle may be possible in a lower density plasma.[12] Numbers of interest based on present technological limitations are given in Sec. IV.

For comparison purposes we examine two axial profiles, a uniform current density and a current density corresponding to the doorstep transformer ratio. We will write $\rho_b(r,y) = \sigma(r)f(y)$, where the radial profile is taken to be a step function, $\sigma(r) = \sigma_0\Theta(a - r)$, σ_0 having the units of charge density. The axial profile $f(y)$ vanishes for $y < 0$ and is instantaneously cut off at $y = L$, so it can be expressed as $f(y)\Theta(y)\Theta(L - y)$. In calculating the electromagnetic components of the field we make the ultrarelativistic approximation, $k_0 = k_p$, in Eqs. (40)–(42) and keep only the lowest order term in γ^{-1} for each component. We can then perform the y integrations and approximate the fields in the three regions, (I) in front of the beam ($y < 0$), (II) within the beam ($0 < y < L$), and (III) behind the beam ($L < y$). The following fields, given by Eqs. (47)–(55), include inductive effects and are presented only as a useful reference. The fields we will be working with are given in Eqs. (56)–(62).

(I) $y < 0$:

$$E_z(r,y) = \frac{2\pi}{\gamma}\int_0^\infty dr'\, r'\sigma(r')\int_0^\infty d\xi \frac{\xi^3}{(k_p^2 + \xi^2)^{3/2}} \times J_0(\xi r)J_0(\xi r')(g_3 - g_1), \tag{47}$$

$$E_r(r,y) = 2\pi\int_0^\infty dr'\, r'\frac{\partial\sigma}{\partial r'}(r')\int_0^\infty d\xi \frac{\xi}{k_p^2 + \xi^2} \times J_1(\xi r)J_1(\xi r')(g_3 - g_1), \tag{48}$$

$$B_\theta(r,y) = \beta E_r(r,y). \tag{49}$$

(II) $0 < y < L$:

$$E_z(r,y) = 4\pi k_p^2\int_0^\infty dr'\, r'\,\sigma(r')I_0(k_p r_<)K_0(k_p r_>) \times \int_0^y dy' f(y')\cos k_p(y - y') + \frac{2\pi}{\gamma}\int_0^\infty dr'\, r'\sigma(r')\int_0^\infty d\xi \frac{\xi^3}{(k_p^2 + \xi^2)^{3/2}} \times J_0(\xi r)J_0(\xi r')(g_3 - g_1), \tag{50}$$

$$E_r(r,y) = 4\pi \int_0^\infty dr'\, r' \frac{\partial}{\partial r'} \sigma I_1(k_p r_<) K_1(k_p r_>) \times \left(k_p \int_0^y dy' f(y') \sin k_p (y-y') - f(y) \right) + 2\pi \int_0^\infty dr'\, r' \frac{\partial \sigma}{\partial r'} \int_0^\infty d\zeta \frac{\zeta}{k_p^2 + \zeta^2} \times J_1(\zeta r) J_1(\zeta r') (g_2 + g_3), \quad (51)$$

$$B_\theta(r,y) = -4\pi\beta \int_0^\infty dr'\, r' \frac{\partial \sigma}{\partial r'} I_1(k_p r_<) K_1(k_p r_>) f(y) + 2\pi \int_0^\infty dr'\, r' \frac{\partial \sigma}{\partial r'} \int_0^\infty d\zeta \frac{\zeta}{k_p^2 + \zeta^2} \times J_1(\zeta r) J_1(\zeta r') (g_2 + g_3). \quad (52)$$

(III) $L < y$:

$$E_z(r,y) = 4\pi k_p^2 \int_0^\infty dr'\, r' \sigma(r') I_0(k_p r_<) K_0(k_p r_>) \times \int_0^L dy' f(y') \cos k_p (y-y') + \frac{2\pi}{\gamma} \int_0^\infty dr'\, r' \sigma \int_0^\infty d\zeta \frac{\zeta^3}{(k_p^2 + \zeta^2)^{3/2}} \times J_0(\zeta r) J_0(\zeta r') (g_4 - g_2), \quad (53)$$

$$E_r(r,y) = 4\pi \int_0^\infty dr'\, r' \frac{\partial \sigma}{\partial r'} I_1(k_p r_<) K_1(k_p r_>) k_p \times \int_0^L dy' f(y') \sin k_p (y-y') + 2\pi \int_0^\infty dr'\, r' \frac{\partial \sigma}{\partial r'} \int_0^\infty d\zeta \frac{\zeta}{k_p^2 + \zeta^2} \times J_1(\zeta r) J_1(\zeta r') (g_4 - g_2), \quad (54)$$

$$B_\theta(r,y) = 2\pi\beta \int_0^\infty dr'\, r' \frac{\partial \sigma}{\partial r'} \int_0^\infty d\zeta \frac{\zeta}{k_p^2 + \zeta^2} \times J_1(\zeta r) J_1(\zeta r') (g_4 - g_2). \quad (55)$$

In writing the fields we have for brevity defined four functions,

$$g_1(\zeta,y) = f(0) e^{\gamma (k_0^2 + \zeta^2)^{1/2} y},$$
$$g_2(\zeta,y) = f(0) e^{-\gamma (k_p^2 + \zeta^2)^{1/2} y},$$
$$g_3(\zeta,y) = f(L) e^{\gamma (k_p^2 + \zeta^2)^{1/2} (y-L)},$$
$$g_4(\zeta,y) = f(L) e^{-\gamma (k_p^2 + \zeta^2)^{1/2} (y-L)}.$$

In their respective regions these functions represent purely decaying inductive fields associated with the switching on and off of the beam current. Except for very diffuse plasmas these terms can be safely ignored, and we can approximate the fields by (I) $y < 0$,

$$E_z = E_r = B_\theta = 0; \quad (56)$$

(II) $0 < y < L$,

$$E_z(r,y) = -4\pi k_p^2 \int_0^\infty dr'\, r' \sigma(r') I_0(k_p r_<) K_0(k_p r_>) \times \int_0^y dy' f(y') \cos k_p (y-y'), \quad (57)$$

$$E_r(r,y) = 4\pi \int_0^\infty dr'\, r' \frac{\partial \sigma}{\partial r'} I_1(k_p r_<) K_1(k_p r_>) \times \left(k_p \int_0^y dy' f(y') \sin k_p (y-y') - f(y) \right), \quad (58)$$

$$B_\theta(r,y) = -4\pi\beta \int_0^\infty dr'\, r' \frac{\partial}{\partial r'} \sigma I_1(k_p r_<) \times K_1(k_p r_>) f(y); \quad (59)$$

(III) $L < y$,

$$E_z(r,y) = 4\pi k_p^2 \int_0^\infty dr'\, r' \sigma(r') I_0(k_p r_<) K_0(k_p r_>) \times \int_0^L dy' f(y') \cos k_p (y-y'), \quad (60)$$

$$E_r(r,y) = 4\pi \int_0^\infty dr'\, r' \frac{\partial \sigma(r')}{\partial r'} I_1(k_p r_<) K_1(k_p r_>) k_p \times \int_0^L dy' f(y') \sin k_p (y-y'), \quad (61)$$

$$B_\theta = 0. \quad (62)$$

Notice that within the beam E_r contains a term $f(y)$ proportional to the bare beam charge. This term, which can be as large or larger than the induced plasma response, represents the branch cut contribution missing from Eq. (19). Given E_r and B_θ within the beam [region (II)] we can write down the radial wakefield that causes beam pinching:

$$W(r,y) = 4\pi \int_0^\infty dr'\, r' \frac{\partial \sigma(r')}{\partial r'} I_1(k_p r_<) K_1(k_p r_>) \times \left(k_p \int_0^y dy' f(y') \sin k_p (y-y') - \frac{f(y)}{\gamma^2} \right). \quad (63)$$

The term proportional to $f(y)/\gamma^2$ represents the self-repulsion of the beam's space charge. This term dominates within a relativistic skin depth of the beam head, meaning that the head of the beam can not be confined by the radial wakefield induced in the plasma. For ultrarelativistic beams this term can be ignored. It is interesting to note that for sufficiently large γ the electrostatic result gives the correct radial wakefield. However, as we shall see in the following paragraphs it is the magnetic field that is responsible for the pinching of the beam, not the electrostatic radial field.

We now consider two specific forms for the axial current profile $f(y)$ and calculate the fields within and behind the beam; we ignore the decaying wakes. We only write down the fields within the beam channel, i.e., for $r \leqslant a$. Outside the beam channel the fields fall off exponentially. The first profile we examine represents a uniform current density along the length of the beam. The second profile corresponds to a current density that is linearly ramped over most of the beam length. For comparison purposes the total charge and peak

density (σ_0) in the two beams is the same. This necessarily means that the pulse length of the ramped beam is longer than that of the uniform profile beam. For the uniform profile, $f(y) = \Theta(y)\Theta(L-y)$, we find that the fields in the two regions, (a) $y \leqslant L$ and (b) $y > L$, are given by

$$y \leqslant L, \quad E_z(r,y) = -(4\pi\sigma_0/k_p)\sin k_p y \times [1 - k_p a K_1(k_p a) I_0(k_p r)]; \tag{64a}$$

$$y > L, \quad E_z(r,y) = -(4\pi\sigma_0/k_p) \times [\sin k_p y - \sin k_p (y-L)] \times [1 - k_p a K_1(k_p a) I_0(k_p r)]; \tag{64b}$$

$$y \leqslant L, \quad E_r(r,y) = -4\pi\sigma_0 a \cos k_p y K_1(k_p a) I_1(k_p r); \tag{65a}$$

$$y > L, \quad E_r(r,y) = -4\pi\sigma_0 [\cos k_p y - \cos k_p (y-L)] \times K_1(k_p a) I_1(k_p r); \tag{65b}$$

$$y \leqslant L, \quad B_\theta(r,y) = -4\pi\sigma_0 a K_1(k_p a) I_1(k_p r); \tag{66a}$$

$$y > L, \quad B_\theta(r,y) = 0. \tag{66b}$$

Note that the maximum accelerating field behind the beam is twice the maximum decelerating field within the beam. This implies a transformer ratio, $R = 2$, and demonstrates the fundamental theorem of beam loading for symmetric current distributions. Physically this low efficiency is attributable to the fact that the axial field within the beam is oscillatory; energy lost by part of the beam to the wakefield is regained by another part of the beam. For this distribution the radial wakefield is

$$W(r,y) = 4\pi\sigma_0 a(\cos k_p y - \beta^2) K_1(k_p a) I_1(k_p r), \tag{67}$$

and the beam pinching oscillates along the length of the beam.

We next consider an axial current profile that leads to a transformer ratio that can be much larger than 2. This requires that the charge distribution within the beam is asymmetric from head to tail. Such a current profile has been investigated by Bane *et al.*,[4] and has become known as the doorstep distribution. In the doorstep distribution the current is uniform for the first quarter plasma wavelength and then rises linearly with a particular slope to its maximum value. (A typographical error for the slope exists in Ref. 4 and is here corrected.) In order to make the total charge of the doorstep profile the same as the charge of the uniform profile the length of the beam must be made to be approximately twice as long as that for the uniform beam. This profile results in an E_z that is uniform throughout most of the beam:

$$f(y) = 1/(1 - \pi/2 + k_p L), \quad 0 \leqslant y \leqslant \lambda_p/4,$$
$$f(y) = (1 - \pi/2 + k_p y)/(1 - \pi/2 + k_p L), \quad \lambda_p/4 \leqslant y \leqslant L. \tag{68}$$

For brevity we let $R_1(r)$ and $R_2(r)$ represent the radial dependencies for E_z, and E_r and B_θ, respectively. These dependencies are of course the same as that found for the uniform profile;

$$R_1(r) = 1 - k_p a K_1(k_p a) I_0(k_p r), \tag{69}$$

$$R_2(r) = k_p a K_1(k_p a) I_1(k_p r). \tag{70}$$

In terms of these functions the fields in the three regions, (a) $0 \leqslant y \leqslant \lambda_p/4$, (b) $\lambda_p/4 \leqslant y \leqslant L$, and (c) $y > L$, are given by

$$0 \leqslant y \leqslant \frac{\lambda_p}{4}, \quad E_z(r,y) = -\frac{4\pi\sigma_0}{k_p} R_1(r) \frac{\sin k_p y}{1 - \pi/2 + k_p L}; \tag{71a}$$

$$\frac{\lambda_p}{4} \leqslant y \leqslant L, \quad E_z(r,y) = -\frac{4\pi\sigma_0}{k_p} R_1(r) \frac{1}{1 - \pi/2 + k_p L}; \tag{71b}$$

$$y > L, \quad E_z(r,y) = \frac{4\pi\sigma_0}{k_p} R_1(r) \times \left(\sin k_p (y-L) - \frac{\cos k_p (y-L)}{1 - \pi/2 + k_p L} \right); \tag{71c}$$

$$0 \leqslant y \leqslant \frac{\lambda_p}{4}, \quad E_r(r,y) = -\frac{4\pi\sigma_0}{k_p} R_2(r) \cos k_p y; \tag{72a}$$

$$\frac{\lambda_p}{4} \leqslant y \leqslant L, \quad E_r(r,y) = 0; \tag{72b}$$

$$y > L, \quad E_r(r,y) = -\frac{4\pi\sigma_0}{k_p} R_2(r) \times \left(\cos k_p (y-L) + \frac{\sin k_p (y-L)}{1 - \pi/2 + k_p L} \right); \tag{72c}$$

$$0 \leqslant y \leqslant \frac{\lambda_p}{4}, \tag{73a}$$

$$B_\theta(r,y) = -\frac{4\pi\beta\sigma_0}{k_p} R_2(r) \frac{1}{1 - \pi/2 + k_p L};$$

$$\frac{\lambda_p}{4} \leqslant y \leqslant L, \quad B_\theta(r,y) = -\frac{4\pi\beta\sigma_0}{k_p} R_2(r) \frac{1 - \pi/2 + k_p y}{1 - \pi/2 + k_p L}; \tag{73b}$$

$$y > L, \quad B_\theta(r,y) = 0. \tag{73c}$$

From the equations for the axial electric field one sees that a large transformer ratio, $R = [1 + (1 - \pi/2 + k_p L)^2]^{1/2}$, is possible for this distribution. It is important to note that the increased transformer ratio has come about through a reduction in the decelerating field within the beam, and not from an increase in the accelerating field behind the beam. In fact, for large $k_p L$ the maximum accelerating field behind the beam is actually smaller than that found for the uniform beam [see Eq. (65)]. For long pulse lengths R can greatly exceed 2. Within the present analysis the pulse length is limited to approximately 40 plasma periods, since for longer pulses the ion dynamics begin to play a role. This then limits the transformer ratio to 80π, or $R \approx 250$. Inclusion of ion dynamics should, however, only increase the plasma wavelength, and R could theoretically be made much larger. For the doorstep distribution the axial field within the beam is totally decelerating. Therefore, unlike the uniform current case, all the energy lost by the beam goes into the wakefield; none is recovered. However, the beam pinching for this profile is not uniform along the beam axis, and this will lead to a deterioration of the beam quality and to a reduction in R. In fact, the pinching is maximum for this case because the radi-

al electric field is zero within the main body of the beam; therefore there is no compensation of the pinching Lorentz force as there is in vacuum. Behind the doorstep the radial wakefield is solely attributable to the azimuthal B field;

$$W(r,y) = -\frac{4\pi\beta^2\sigma_0}{k_p} R_2(r) \frac{1-\pi/2+k_p y}{1-\pi/2+k_p L} + \text{terms } O(\gamma^{-2}). \tag{74}$$

The radial dependence R_2 determines whether the pinching occurs throughout the whole beam or only on the edge. This is related to the return current induced in the plasma, and is discussed in the following section. The pinching process is obviously very nonlinear and can only be followed numerically. In Sec. III we present simulation results that show how pinching affects the beam and its wakefield.

IV. SELF-CONSISTENT EVOLUTION OF THE DRIVING BUNCH

The analysis presented so far has yielded the longitudinal and transverse wakefields assuming that the charge and current profiles of the driving bunch remain fixed. It was found that the transverse wakefield can be comparable in magnitude to the longitudinal wakefield. If tailoring of the driving bunch to optimize the transformer ratio is to make sense, the driving beam must lose most of its energy before the transverse wakefield alters the profile of the tailored bunch. A conservative estimate of the conditions necessary for maintaining the profile of the driving bunch can be made by comparing the ratio of the longitudinal wakefield to the transverse wakefield within the beam. Aside from some factors that depend on the detailed axial profile of the bunch this ratio is given by

$$\frac{W}{E_z} \sim \frac{R_2(r)}{R_1(r)} = \frac{k_p a K_1(k_p a) I_1(k_p a)}{1 - k_p a K_1(k_p a) I_0(k_p r)}. \tag{75}$$

For beam pulse shaping to have an effect this ratio must be small. The doorstep profile makes this ratio larger by the transformer ratio.

For beams in which the radius is small ($k_p a \ll 1$) we can expand the Bessel functions to obtain

$$R_1 \simeq k_p^2 a^2 [\ln(k_p a/2) + \gamma], \quad R_2 \simeq k_p r,$$

where γ is Euler's constant ($\gamma = 0.577\,21...$). Hence,

$$\frac{R_2}{R_1} \simeq \frac{r}{a} \frac{1}{k_p a[\ln(k_p a/2) + \gamma]}. \tag{76}$$

Thus for small beam radii the transverse wakefields will always dominate the longitudinal wakefield and pulse tailoring will be ineffective (except near $r = 0$). Assuming that both $k_p a \gg 1$ and $k_p r \gg 1$ we can use the asymptotic expansions of the Bessel functions to obtain

$$R_1 \simeq 1 - (a/4r)^{1/2} e^{-k_p(a-r)},$$

$$R_2 \simeq (a/4r)^{1/2} e^{-k_p(q-r)},$$

so that

$$\frac{R_2}{R_1} \simeq \frac{(a/4r)^{1/2} e^{-k_p(a-r)}}{1 - (a/4r)^{1/2} e^{-k_p(a-r)}}. \tag{77}$$

Therefore we find that even for large beams the transverse wakefield is comparable to the accelerating field at the beam edge, $r = a$. However, if the beam is large enough this ratio can be made small everywhere except within a couple of skin depths (c/ω_p) of the beam edge. The difference between the small and large radii beams is attributable to a difference in the return currents induced in the plasma. Using Ohm's law, $\partial \mathbf{J}_p/\partial t = \omega_p^2/4\pi \mathbf{E}$, it is easy to show that for the doorstep current profile the ratio of the induced current to the beam current behind the doorstep is given by

$$\frac{J_p}{J_b} = \frac{1-\pi/2+k_p y}{1-\pi/2+k_p L} R_1(r). \tag{78}$$

One then sees that for small radii beams J_p/J_b effectively vanishes, while for large beams the induced current penetrates a couple of skin depths into the beam. Thus we are led to the conclusion that pulse shaping will quickly become ineffective due to self-forces unless the beam is large ($\omega_p a/c \gg 1$).

We now give an estimate of the current required to result in an accelerating field that approaches the wave-breaking limit. From Eq. (71c) the electric field behind the driving bunch is given by

$$E = G(r)(4\pi\sigma_0/k_p), \tag{79}$$

where $G(r)$ is a geometrical factor of order 1 and σ_0 is the peak charge density in the driving bunch. This equation can be expressed in terms of dimensionless variables as follows:

$$eE/mc\omega_p = [4(eI/mc^3)]/(\omega_p a/c)^2, \tag{80}$$

where I is the peak current in the beam which is assumed radially uniform. We recognize that the dimensionless quantity on the left-hand side of the equation is the peak electric field normalized to the wave-breaking field in the plasma. In order to take advantage of the large accelerating gradients that a plasma can support, it is desirable to have this quantity near one. However, the requirement that the beam be large in order to maintain pulse tailoring means that the peak current must be large. From this equation, assuming $\omega_p a/c = 10$ is adequate to avoid beam pinching, we find that in order to approach the wave-breaking limit a peak current of 425 kA is required. This result is independent of the actual beam radius or the plasma density. As we will see from the simulation results, $\omega_p a/c$ may need to be much larger than 10. The requirement of large currents makes it very difficult to achieve the maximum accelerating field possible in a plasma. Furthermore, these large currents tend to make the driving beam unstable to filamentation and hose instabilities. Going to a higher energy beam will not alleviate the problem of filamentation; in fact it will become worse. The time for filamentation to occur[13] scales as $\tau_f \sim \gamma^{1/2}$; the time for the beam to lose a certain fraction of its energy, say ΔE, scales as $\tau_{\Delta E} \sim \gamma$. To beat the filamentation instability one would require that $\tau_f/\tau_{\Delta E}$ increase with increasing γ. However, $\tau_f/\tau_{\Delta E} \sim \gamma^{-1/2}$, meaning that filamentation occurs faster than beam energy loss with increasing energy.

In order to test these conclusions and to explore more fully the self-consistent evolution of the driving beam in a plasma wakefield accelerator, the system has been simulated with the particle-in-cell model ISIS.[7] Simulations have been performed with immobile ions and particle plasma electrons

and particle beam electrons. However, for the parameters of interest the plasma electrons act as a linearized cold fluid. Thus a much more quiescent and cost effective way of treating the background plasma is to model it as a linearized cold fluid. To do this in ISIS the current density $\mathbf{J}_p$ attributable to the plasma electron evolves according to the simple prescription

$$\frac{\partial \mathbf{J}_p}{\partial t} = \frac{\omega_p^2}{4\pi}\mathbf{E}. \tag{81}$$

This equation is finite differenced in time and is applied locally on the two-dimensional finite difference grid. This current density is then added to the current density due to the beam particles and the result is used as a source term in Maxwell's equations in the usual way. ISIS does not require a separate array of charge density because a Poisson correction is unnecessary.[14] This procedure accurately models the plasma dynamics as long as $eE/mc\omega_p < 1$, while the full nonlinear and self-consistent evolution of the beam is treated by the usual particle-in-cell method.

The beam dynamics for a small beam ($\omega_p a/c = 2$) from a simulation are shown in Fig. 2. The beam particles are injected from the left-hand boundary to give a doorstep transformer profile, with a transformer ratio of about ten. This means the total pulse length τ is given by $\omega_p \tau = 10.52$. The peak injected beam density is $n_b/n_p = 0.2$, and the beam energy $\gamma mc^2 = 20$. The finite difference grid consists of 12 500 cells, each $0.4c/\omega_p$ on a side. The time step is $0.2\omega_p^{-1}$. The figure consists of ten snapshots of the beam particle positions superimposed. The first snapshot is taken at $\omega_p t = 20$, and succeeding snapshots are taken at intervals of $\omega_p t = 20$. Even as early as $\omega_p t = 20$ the driving bunch can be seen to have begun to pinch as a result of the transverse wakefield. By the second snapshot at $\omega_p t = 40$, the pinching has become quite severe. Similar strong pinching effects have been observed in two-dimensional Cartesian simulations.[11] The fact that the back of the beam pinches severely while there is little or no pinching of the front of the beam pulse means that the doorstep pulse tailoring is completely destroyed by this time. The other snapshots in Fig. 2 show the subsequent evolution of the pulse, which pinches to a much smaller radius (except near the front) than originally injected. The phase space for the bunch is shown in Fig. 3. If the doorstep profile were maintained all the particles except

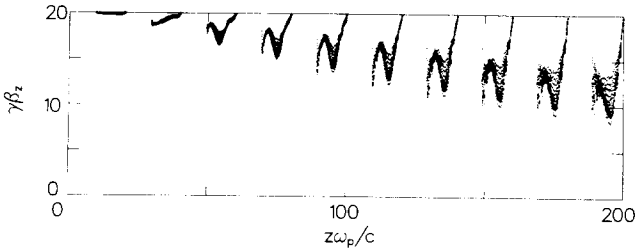

FIG. 3. Phase space for the beam shown in Fig. 1. The self-consistent modification of the beam profile results in nonuniform deceleration of the driving beam and hence inefficient accelerator performance.

those in the first quarter wavelength would lose their energy at the same rate. As can be seen from Fig. 3 the energy loss has become nonuniform by the second snapshot ($\omega_p t = 40$), before the beam has lost even 10% of its energy. The subsequent phase space snapshots show a very nonuniform deceleration of the beam, which means a loss of accelerator efficiency.

Figure 4 shows the same set of snapshots as Fig. 2 for a simulation with the beam radius ten times larger ($\omega_p a/c = 20$). All other parameters are the same. As predicted by the analysis, initially the pinching occurs only near the beam edge. Comparing Fig. 4 with Fig. 2 shows that the larger beam maintains its integrity longer than the smaller beam. However, later the large beam is seen to undergo a strong filamentation instability. The current does not scale out of the simulation parameters: for the small beam the peak beam current is 3.4 kA. The larger beam has the same current density and hence 100 times the total current, or a peak current of 340 kA. This current is near the Alfvén limit for a $\gamma = 20$ beam. It can be expected that this large current would produce not only filamentation instabilities, but also a hose instability in a real beam. The phase space for this simulation is shown in Fig. 5. The first few snapshots show a more uniform deceleration of the beam than the small beam calculation shown in Fig. 3. However, later the deceleration has become nonuniform as a result of the filamentation instability.

A weak trailing bunch ($n_b/n_p = 0.01$) was injected immediately following the driving beam in this simulation. Fig-

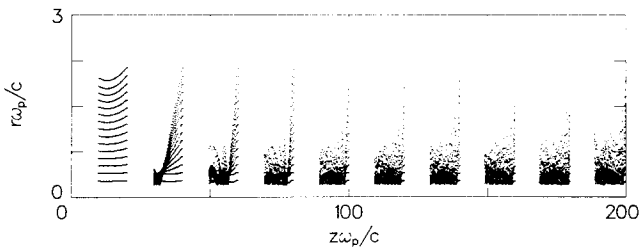

FIG. 2. Superposition of ten snapshots of the driving beam from a particle-in-cell simulation. The beam is shown every $\omega_p \Delta t = 20$. The initial radius a of the injected beam is $\omega_p a/c = 2$. The beam rapidly pinches as a result of transverse wakefields and the injected current profile is modified.

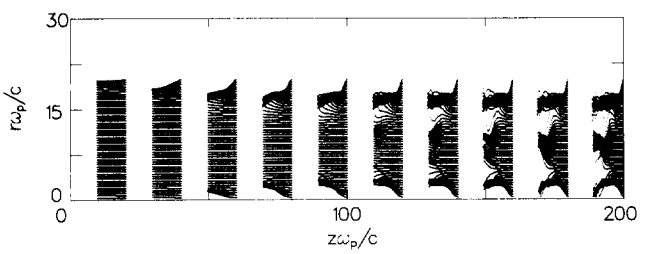

FIG. 4. Snapshots of the beam particles for a simulation with a large radius beam ($\omega_p a/c = 20$). Self-consistent pinching is less pronounced than in the simulation results shown in Fig. 1. A strong filamentation instability is seen in the later snapshots.

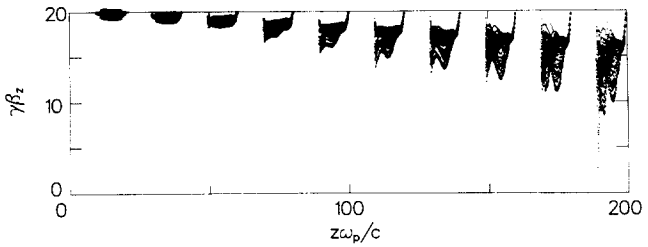

FIG. 5. Phase space snapshots for the beam shown in Fig. 3. Uniform deceleration is observed in the earlier snapshots. However, the filamentation instability degrades accelerator performance later.

ure 6 shows the configuration snapshots for these particles. The trailing bunch was chosen to be exactly one plasma wavelength long so that it samples both accelerating and decelerating portions of the axial electric field and focusing and defocusing regions of the transverse wakefield. The portions of the beam that experience the defocusing transverse wakefield are quickly pushed out to the conducting drift tube. The portions of the beam near the head and tail of the bunch that experience focusing remain confined and track behind the driving beam. However, as a result of the filamentation instability experienced by the driving beam these are not uniformly accelerated. Portions of the trailing bunch are found to be accelerated to over 35 MeV, however, the nonlinear character of the focusing force leads to a very large emittance in the accelerated particles (transverse energy comparable to longitudinal energy).

These studies suggest that the self-consistent transverse motion of the driving bunch makes the highly desirable pulse tailoring impossible to maintain. At higher voltages, the beam pinching will be slower because relativistic effects make the beam more massive and hence stiffer. However, the beam must also travel farther in order to lose the same fraction of its energy. Both of these effects scale as the Lorentz factor γ. What matters for an accelerator is how fast the pinching occurs relative to the beam energy loss rate. Thus the pinching cannot be ameliorated by using higher energy beams.

An alternative method of preventing beam pinching is to apply an external axial magnetic field. Preliminary simulations of the plasma wakefield accelerator including a magnetic field indicate that pinching can be reduced in this case, but the details have not yet been worked out.[15] One can provide a rough estimate of the magnetic field strength that is needed: the cyclotron frequency Ω_c must exceed the beam plasma frequency by a factor of 3–5. Typically ω_b will be somewhat smaller than the plasma frequency ω_p in order to avoid wave breaking. Therefore a conservative estimate of the magnetic field can be obtained by assuming that $\Omega_c > \omega_p$. To get an accelerating gradient of 1 GeV/m, the plasma frequency must be at least $\omega_p = 5.64\times 10^{11}$ sec^{-1}, which means a magnetic field, $B_z \approx 30$ kG must be impressed along the entire length of the accelerator in order to avoid beam pinching. Higher gradients would require even higher magnetic fields to guide the beam. The complication of applying a magnetic field of tens of kilogauss along the accelerator places a severe technological restriction on the accelerating gradient that can be obtained in a plasma wakefield accelerator.

If the beam density is reduced so that the accelerator is operated well below wave breaking ($eE/mc\omega_p \ll 1$), Eq. (80) shows that less current would be needed to avoid beam pinching. However, one still requires that the driving beam must be cut off in a time short compared with ω_p^{-1}. Assuming the technology can be developed to do this in 1–10 psec, the maximum accelerating gradient would be limited to between 200 MeV/m and 2 GeV/m. Operating a factor of 10 below this limit would make the plasma wakefield only marginally better than existing rf accelerator technology.

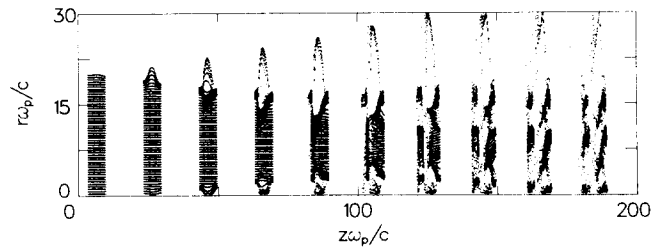

FIG. 6. Snapshots of a test-particle trailing bunch one wavelength long following the driving bunch in Fig. 3. Transverse wakefields lead to strong radial perturbations in this beam.

V. CONCLUSION

The electromagnetic wakefields generated by a relativistic, azimuthally symmetric current distribution passing through a cold, unmagnetized plasma have been derived in full generality [Eqs. (47)–(55)]. To lowest order in γ^{-1} these fields are given by Eqs. (56)–(62). The radial wakefield, $\mathbf{W} = \mathbf{r}(E_r - \beta B_\theta)$, that results in the self-consistent pinching of the beam has been calculated in Eq. (63). The electromagnetic fields and radial wakefield have been evaluated for a current distribution corresponding to the doorstep transformer ratio for the plasma wakefield accelerator concept (PWFA) [Eqs. (71)–(74)]. Simulations of the PWFA confirm that the pinching attributable to the radial wakefield is so severe that the doorstep current profile cannot be maintained. Beam pinching has been found to be most deleterious for small radii beams ($a\omega_p/c \ll 1$), while large radii beams exhibit strong filamentation instabilities. Increasing γ does not alleviate the problems associated with filamentation.

ACKNOWLEDGMENTS

We would like to thank W. R. Shanahan for useful discussions on this topic, and thank Catherine MacDonald for a careful proofreading of the manuscript.

[1] P. Chen, R. W. Huff, and J. M. Dawson, Bull. Am. Phys. Soc. **29**, 1355 (1984); P. Chen, J. M. Dawson, R. W. Huff, and T. Katsouleas, Phys. Rev. Lett. **54**, 693 (1985).

[2]R. D. Ruth, A. Chao, P. L. Morton, and P. B. Wilson, Part. Accel. **17**, 171 (1985).
[3]A. W. Chao, in *Physics of High Energy Particle Accelerators: AIP Conference Proceedings No. 105* (AIP, New York, 1983), p. 353.
[4]K. L. F. Bane, P. Chen, and P. B. Wilson, IEEE Trans. Nucl. Sci. **32**, 3524 (1985).
[5]P. Chen and J. W. Dawson, in *Laser Acceleration of Particles, AIP Proceedings No. 127* (AIP, New York, 1985), p. 201.
[6]See for example, J. D. Jackson, *Classical Electrodynamics* (Wiley, New York, 1975), Chap. 13.
[7]G. R. Gisler and M. E. Jones, Bull. Am. Phys. Soc. **29**, 1208 (1984).
[8]J. L. Cox, Jr. and W. H. Bennett, Phys. Fluids **13**, 182 (1970).
[9]I. H. Sneddon, *The Use of Integral Transforms* (McGraw-Hill, New York, 1972), Chap. 5.
[10]I. S. Gradshteyn and I. M. Ryzhik, *Table of Integrals, Series and Products* (Academic, New York, 1965).
[11]T. Katsouleas, Phys. Rev. A **33**, 2056 (1986).
[12]J. B. Rosenzweig, D. B. Cline, R. N. Dexter, D. J. Larson, A. W. Leonard, K. R. Mengelt, J. C. Sprott, F. E. Mills, and F. T. Cole, in Ref. 5, p. 226.
[13]K. Molvig, Phys. Rev. Lett. **35**, 1504 (1975).
[14]G. Gisler and M. E. Jones, in *Proceedings of the 11th International Conference on Numerical Simulations of Plasma* (Institut de Recherche de'Hydro-Quebec, Montreal, Quebec, 1985), Article No. 1.B.01.
[15]R. K. Keinigs, B. DeVolder, and M. E. Jones, Bull. Am. Phys. Soc. **30**, 1615 (1985).